October 2020

Assessing Many-Body van der Waals Contributions in Model Sorption Environments

Matthew K. Mostrom
University of South Florida

Assessing Many-Body van der Waals Contributions in Model Sorption Environments

by

Matthew K. Mostrom

A thesis submitted in partial fulfillment
of the requirements for the degree of
Master of Science
Department of Chemistry
College of Arts and Sciences
University of South Florida

Major Professor: Brian Space, Ph.D.
Arjan van der Vaart, Ph.D.
Shengqian Ma, Ph.D.
Preston Moore, Ph.D.

Date of Approval:
October 20th, 2020

Keywords: Monte Carlo, molecular dynamics, potential energy, electronic structure, porous materials, gas sorption

Table of Contents

List of Tables

List of Figures

Abstract

The energy used in the separation and purification of small volatile atoms and compounds represents a sizable fraction of the world's energy consumption as a whole[1]. Noble gases in particular represent a unique challenge as their separation currently relies on distillation methods that work by virtue of small differences in the density of their pure phases. Highly porous Metal-Organic Materials (MOMs) offer a cheaper, more efficient alternative to cryogenic distillation, and studying their properties using various simulation methods has become an important and active area of research. The family of Potentials with "High Accuracy, Speed and Transferability" (PHAST) have been demonstrated to be unphysically repulsive at short separation distances due to the limitations of the Lennard-Jones 12-6 function. The updated PHAST model, herein "PHAHST" has evolved to use a more fundamentally grounded repulsion/ dispersion potential form, including exponential repulsion, C_6, C_8, and C_{10} dispersion parameters and dispersion-repulsion damping functions. This new functional form, herein PHAHST, is of the Tang-Toennies type, and is shown to excel at modeling sorbates in heterogeneous environments such as those encountered within nanoporous media[2]. This improvement to the potentials reduces the total number of sites of previous models, offering less cumbersome computational cost when using them. Modeling polarization through the use of induced dipoles and representing the permanent electrostatics as point charges is retained. The choice of parameter mixing rules has also been updated, retaining the use of arithmetic averaging for sigma, but adopting a more sophisticated rule for epsilon. Verification and validation of the new model is performed on small ($N \leq 7$) rare-gas clusters composed of helium and neon atoms. High

level ab initio calculations (CCSD(T) using aug-cc-pVTZ/QZ basis functions with extrapolation to the complete basis set limit) are employed to calculate the energy profile of an incident adsorbing particle. Many-body van der Waals (vdW) effects are compared, including Axilrod-Teller-Muto (AT) and coupled-dipole.

1 Introduction

The paradigm under which the modelling of sorbate interactions in porous materials is performed is one of the current frontiers of modern computational chemistry. The study of small-molecule adsorption into highly heterogeneous environments found in the pores of porous coordination polymers (PCPs) is of great interest to many industries for a multitude of purposes, in particular, volatile gas storage, catalysis, and gas separation. In 2005, it was estimated that at least 10-15% of the world's total energy output was used solely in the application of chemical separations. About 45% of the energy used for the processes comprising that figure were cryogenic distillation.[1] This represents an opportunity to find more efficient solutions to these problems using emerging technologies. Materials such as MOMs are poised for use in this role due to their potential for size- and polarizability-selective adsorption.[2–4]

The activity of PCPs is governed by their internal geometries and the access that guest molecules have to specific moieties within them. They are highly porous structures whose scaffolding comprises a network of organic ligands (or "linkers") that attach themselves to central metal or semiconductor atom nodes, forming a regularly repeating crystal structure.[5–7] These pores can be tuned and adjusted for size selectivity,[8] post-synthetic pore modification, and flexibility with environmental parameter changes such as adsorbent gas pressure. This affords vast potential for real and theoretical materials to be explored.

The practical description of these environments and their potential energy surfaces is a particularly challenging and rich field of study, as the interactions which dominate the dynamics of adsorption are strongly influenced by vdW interactions which are not well-represented in modern classical modelling. The industry-standard in most molecular dynamics (MD) simulations to rep-

resent repulsion and dispersion is to use the 6-12 Lennard-Jones potential as the principal (or sole) vdW term.[9–11] This vdW model under-represents the attractive region of the Born-Oppenheimer PES, while the repulsive region is overestimated. This potential is chosen because of its low computational cost and its generally sufficient performance in systems which are not dominated by vdW interaction contributions. However, this leaves a space to be filled by a potential form that is computationally tractable with an underlying form is based on a rationally-explained theoretical basis.[12]

In much of classical modelling, only the effects of the interactions between pairs of particles are considered when calculating the potential energy of a system. This is because it is computationally feasible and yields a result that captures most of the energetics of the system, but also because there is no general closed-form solution to calculating the dynamics of an N-body system where $N>2$, and approximations must instead be used. A common correction is to calculate and add an approximation to the 3-body energy. This can be implemented in a number of ways but in this study, only two methods will be considered for evaluation of the vdW energy: Axilrod-Teller-Muto[13] and coupled-dipole polarizability.[14–16]

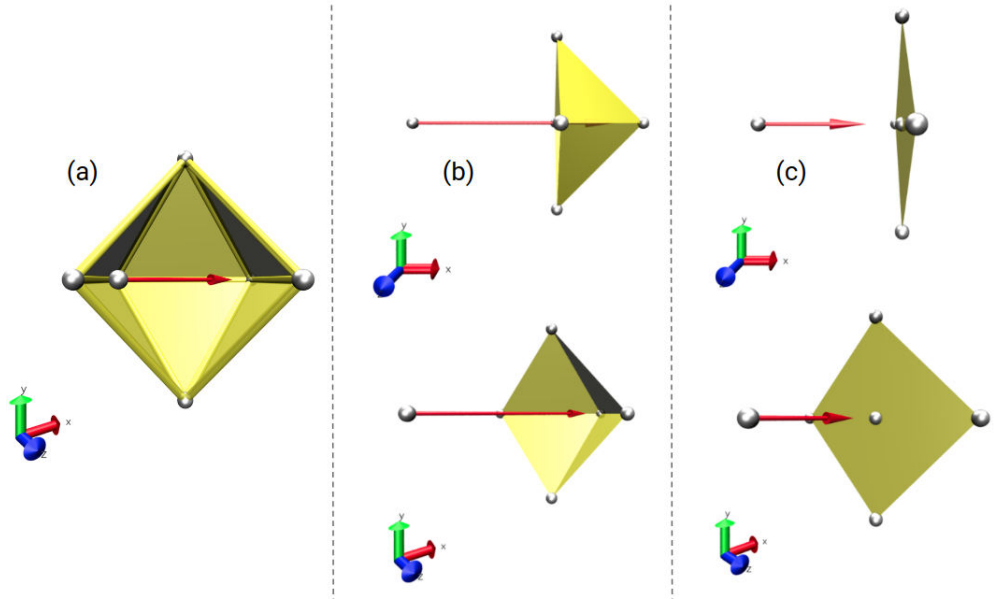

Figure 1: The nanostructures considered in this study: (a) cage, (b) pock, (c) wall. The atom at the tail of the arrow is referred to as the “adsorber” or ”mover” atom, and the atoms that make up the nanostructures are known as the “nanostructure” atoms.

2 Methods

Nanostructures

First, four nanostructure coordinate sets were chosen to represent characteristic motifs one might find in sorption sites of a coordination polymer, and include four different nanostructures: cage, pocket, ring, and wall (Fig. 1). The nanostructures are all made from helium, whereas both helium and neon were used for the mover atom. This was chosen due to restrictions of computational resources, as CCSD(T) scales as O(N^7) with system size. In every nanostructure except the ring motif (c), the adsorbing atom's path directly overlaps with the atomic center of a nanostructure atom. With the ring structure, the adsorbing atom passed through the center of the ring, resembling the passage of a sorbate through the channel of a porous material.

Ab initio evaluation of the single-point energy of each structure was calculated using the CCSD(T) package featured in the ORCA quantum chemistry suite.[17,18] Basis sets used were aug-cc-pVnZ[19,20] (n=3,4,5,6) GTO's and energies were obtained using the minimized Hartree-Fock determinant in the higher of the two basis sets used in a given run. Correlation energies were obtained through extrapolation to the complete basis set.[21] The SCF portion was taken as the minimized Fock matrix of the larger of the two bases. These basis sets were chosen because of their diffuse intermolecular functions, the consideration to emphasizing polarization, and their intended use for extrapolation to the complete basis set limit. For the evaluation of the trimer N-body decomposition, aug-cc-pV5z/6z bases were used whereas for the nanostructures, aug-cc-pV3Z/4Z bases were used due to computational resource restrictions.

Many-body effects were compared to CCSD(T) results of N-body decomposition. This was achieved through counterpoise of the atomic clusters with their successively higher-order terms[22] which were then compared to classical models fit to *ab initio* data using MPMC (Massively Parallelized Monte Carlo).[23] Models include PHAHST,[12] PHAHST + Axilrod-Teller-Muto,[13] PHAHST + coupled dipole vdW,[15,16] and Lennard-Jones.

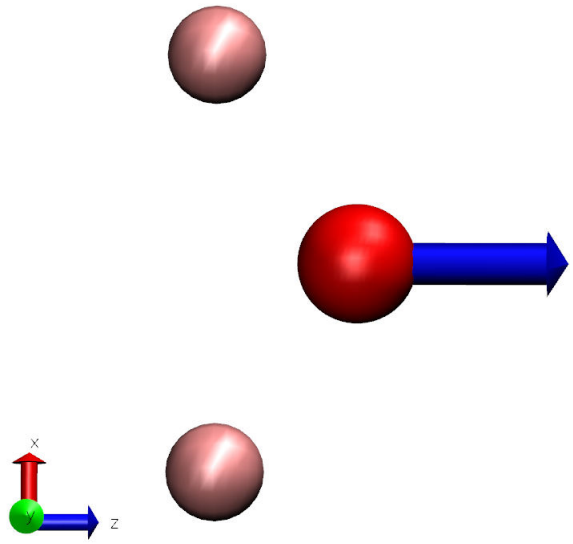

Figure 2: A trimer of noble gas atoms is used to verify the non-additive many-body contributions to the potential surface. In the cases examined, both atoms on the left were fixed heliums at their dimer minimum distance, and the red atom on the right (He in one case and Ne in the other) is used to scan the PES at 0.1 Angstrom intervals.

The energy decomposition was done using a counterpoise scheme which begins with the explicit treatment of all atoms and electrons of the system being considered with CCSD(T) in the aug-cc-pVTZ/QZ bases. Also computed are the unique combinations of single, pair, triplet, N-tuplet configurations of the same system. The contributions of each N-body potential is calculated in the following manner:[22]

$$U^{2b}_{He(i)\cdots He(j)} = E_{He(i)\cdots He(j)} - (E_{He(i)} + E_{He(j)}) \tag{1}$$

$$U^{3b}_{He(i)\cdots He(j)\cdots He(k)} = E_{He(i)\cdots He(j)\cdots He(k)} - U^{2b}_{He(i)\cdots He(j)\cdots He(k)} - (E_{He(i)} + E_{He(j)} + E_{(k)}) \tag{2}$$

and so on, where

$$U^{2b}_{He(i)\cdots He(j)\cdots He(k)} = U^{2b}_{He(i)\cdots He(j)} + U^{2b}_{He(i)\cdots He(k)} + U^{2b}_{He(j)\cdots He(k)} \tag{3}$$

Higher order terms are computed in a similar manner by subtracting lower-order configurations from the highest-order, N-atom system. This is done by a process called ”ghosting”, which involves

excluding the electrons of a ghosted atom from being simulated but still considering their orbital bases for the non-ghosted electrons to interact with.

3 Potential Forms

The form of the PHAHST potential is the following:

$$U = U_{rep} + U_{disp} + U_{ES} + U_{pol} \tag{4}$$

Where U_{rep} is the electronic repulsion energy caused by the Pauli principle and consequent descreening of the nuclei as inter-nuclear separation becomes smaller:

$$U_{rep} = \Sigma_{i \neq j} \frac{F_0}{\beta_{ij}} \exp\left[\beta_{ij}(r_{ij} - \rho_{ij})\right] \tag{5}$$

Exponential repulsion is fitted with the parameters β_{ij} and ρ_{ij},which are the fitted range parameter of the electronic repulsion related to the range of overlap between electrons of the two atoms and the distance at which the repulsive force is equal to F_0. F_0 is defined as 10^{-3} a.u. to allow for practical distance parameter fitting. Note that $f_n(r_{ij}, \beta_{ij})$ is a damping function which ensures the dispersion goes to zero at $r = 0$ and therefore does not infinitely increase, creating a singularity. It has the form:

$$f_{2n}(\beta, r_{ij}) = 1 - e^{-\beta r_{ij}} \sum_{k=0}^{2n} \frac{(\beta r_{ij})^k}{k!} \tag{6}$$

U_{disp} is the dispersion energy:

$$U_{disp} = -f_6(r, \beta_{ij}) \frac{C_6}{r^6} - f_8(r, \beta_{ij}) \frac{C_8}{r^8} - f_{10}(r, \beta_{ij}) \frac{C_{10}}{r^{10}} \tag{7}$$

The C_6 and C_8 dispersion parameters from Eq. 4 were first fit to atomic polarizabilities at imaginary frequencies[12,24] and Gauss–Legendre quadrature.[25] They were then later fit alongside the β_{ij}, ρ_{ij}, and ω_0 parameters through fitting to the Born-Oppenheimer pair potential surface (i.e.

CCSD(T)/aug-cc-pVTZ/QZ + CBS extrapolation[17,18]). We do not calculate higher order dispersion coefficients in the same way as the C6 and C8 parameters due to the need for large basis sets and large angular frequencies. Instead, we recursively calculate the C10 coefficient using the method presented by Thakkar et al.:[26]

$$C_{10} = \frac{49}{40}\frac{C_8^2}{C_6} \tag{8}$$

It should be noted that the β in f_{2n} is the same parameter used in U_{rep}, as both characterize the same electronic overlap phenomenon.

U_{ES} is the electrostatic energy given by Coulomb's law, and U_{pol} is the many-body polarization given by:

$$U_{pol} = -\frac{1}{2}\sum_{i=1}^{N} \overrightarrow{\mu}_i^{ind} \cdot \overrightarrow{E}_i^{stat} \tag{9}$$

as previously defined in earlier work,[16] where $\overrightarrow{\mu_i}$ is the induced dipole moment of atom i, and $\overrightarrow{E_i}$ is the static electric field of the atomic cluster partial charges. Modeling polarization through the use of induced dipoles and representing the permanent electrostatics as point charges is retained from the previously defined PHAST force-field[27,28] using the Thole-Applequist induced polarization method.[29]

Axilrod-Teller-Muto Three-Body van der Waals

The Axilrod-Teller-Muto potential was the first third-order perturbative approximation of the van der Waals force between three bodies via induced dynamic dipole interactions.[13] It been found to be a useful dispersion correction term because it, combined with the two-body interactions, reproduces most of the *ab initio* energy of a system. Due to the progressively smaller contributions made by higher-order terms at thermal intermolecular distances, higher-order terms can sometimes be neglected and have the fidelity of the model remain reasonably accurate.

It is given by the form:

$$V_{ijk} = C_9[\frac{1 + 3cos\gamma_i cos\gamma_j cos\gamma_k}{(r_{ij}r_{jk}r_{ik})^3}] \tag{10}$$

where C_9 is a three-dipole dispersion coefficient calculated from an extrapolation of the C_6 two-dipole term which is derived from the integration of dynamic dipole polarizabilities at imaginary frequencies.[12,30] The homonuclear three-body dispersion term is given by:

$$C_9^{(iii)} = \frac{3}{4}\alpha_{(i0)}C_6^{(ii)} \tag{11}$$

where $\alpha_{(0)}$ is the static atomic polarizability of atom i and $C_6^{(ii)}$ is the homonuclear two-dipole dispersion coefficient.[31] An approximated mixing rule for the C_9 dispersion term is given by:

$$C_9^{ijk} = \frac{3(\alpha_i^3\alpha_j^3\alpha_k^3)^{1/3}}{(\frac{\alpha_i^3}{C_9^i}) + (\frac{\alpha_j^3}{C_9^j}) + (\frac{\alpha_k^3}{C_9^k})} \tag{12}$$

where i, j, k are atom labels.

Coupled-Dipole Many-Body van der Waals

Axilrod-Teller-Muto offers a useful first pass at describing the importance and necessity of many-body interactions in close- and intermediate-range interactions. However, when considering systems with highly heterogeneous regions such as the adsorption site within the pore of a MOF, higher order terms become increasingly important to finding the correct sorbate orientations and configurations; small changes in a sorbate's total interaction energy can have qualitatively large effects in its behavior and placement within a given material. The coupled-dipole approach to induced many-body van der Waals effects makes the problem of electron correlation into a 3N eigenvalue diagonalization or an equivalent self-consistent determination of 3N linear equations.

We first consider the total question of polarization. According to the Thole-Applequist model

of polarization:

$$\begin{aligned}\overrightarrow{u_i} &= \alpha_i(\overrightarrow{E}_i^{stat} + E_i^{ind}) \\ &= \alpha_i(\overrightarrow{E}_i^{stat} - \sum_j \hat{\mathbf{T}}_{ij}\overrightarrow{E_j})\end{aligned} \tag{13}$$

where $\overrightarrow{u_i}$is the total polarized dipole, i, j are other atoms (1,2,...,N-1), $\hat{\mathbf{T}}_{ij} = \nabla\nabla\frac{1}{r_{ij}} = \frac{1}{r_{ij}^3} - \frac{3\overrightarrow{r}\otimes\overrightarrow{r}}{r_{ij}^5}$ (the dipole interaction tensor), and $\overrightarrow{E}_i^{stat}$ is the electric field generated by the partial charges of the system. When considering the choice of atoms looked at in this paper, the static electric field, $\overrightarrow{E}_i^{stat}$ = 0, leaving us with only the expression for the induced dipole van der Waals forces, E_i^{ind}, to be considered.

Substituting the vectors in Eq. 13 for index notation, it can rewritten as:

$$u_i^m = \alpha_i(E_i^m - \sum_{j,n} T_{ij}^{mn} u_j^n) \tag{14}$$

where m,n are indicies corresponding to x, y, and z, respectively. After some rearrangement, we are left with:

$$\sum_{j,n}(\frac{1}{\alpha_i}\delta_{ij}\delta mn + T_{ij}^{mn})u_i^n = E_i^m. \tag{15}$$

Considering only the induced dipole interactions, $E_i^m = 0$, and the substitution for α_i can be made:

$$\begin{aligned}\sum_{j,n}(\frac{\omega_i^2 - \omega_{i0}^2}{\alpha_{i0}\omega_{i0}^2}\delta_{ij}\delta mn + T_{ij}^{mn})u_j^n = 0 \\ \sum_{j,n}(\frac{1}{\alpha_{i0}}\delta_{ij}\delta_{mn} + T_{ij}^{mn})u_j^n = \sum_{j,n}\frac{\omega_i^2}{\alpha_{i0}\omega i0}\delta_{ij}\delta_{mn}u_j^n\end{aligned} \tag{16}$$

arriving at the eigenfunction formulation:

$$\sum_{j,n}(\omega_{i0}\delta_{ij}\delta_{mn} + T_{ij}^{mn})u_j^n = \omega_i^2 u_i^m \tag{17}$$

This gives rise to 3N independent harmonic oscillators with frequency ω_{i0}.[32] Each mode of oscillation, represented by eigenvector $\overrightarrow{u}_i$, has a ground state energy $E = \frac{1}{2}\hbar\omega_i \coth \frac{\hbar\omega_i}{2k_bT}$ at non-zero temperatures.[33] We thus find that the total van der Waals energy to be the sum of the energies of these oscillators:

$$U_{vdW} = \frac{\hbar}{2}\sum_{i}^{3N}\omega_{i0}\coth\left(\frac{\hbar\omega_i}{2k_bT}\right). \tag{18}$$

Classical Model Parameter Fitting

The PHAHST-style models require determination of several parameters for each unique atom type used, including the repulsion parameters β_{ij} and ρ_{ij}, Tang-Toennies dispersion coefficients C_6 and C_8, static dipole polarizability α_i, and the characteristic atomic frequency ω_{i0}. Due to the vast parameter space to be fit, it was necessary to fix as many of them as possible in physically-grounded theory before fitting. The dispersion coefficients and α_i were fit using the Williams-Stone-Misquitta (WSM) technique as implemented in CamCASP.[12,34–36] Once determined, they were further fit to the CCSD(T) dimer together with the exponential repulsion terms and, in the case where many-body corrections were used, with those terms, as well. The ratio between the dispersion coefficients and the characteristic frequency was retained in fitting by choosing to scale each of them by the same amount at each step in the Monte Carlo fitting runs. The repulsion parameters β_{ij} and ρ_{ij} were chosen to be fit to the CCSD(T) potential surface with little loss of model quality. Classical models were fit using the Monte Carlo simulation package, MPMC,[23] in a least-squares manner. The *ab initio* data used was derived from a counterpoise extrapolation[18] to the complete basis set using aug-cc-pVTZ/QZ bases concerning correlation energy and the energy of the Fock determinant of the larger of the two bases.

Models Used

Described below are the final parameter values after fitting to the coupled cluster dimer surface using the aug-cc-pVTZ/QZ basis sets:

Table 1: Helium model parameters. Special parameters not listed include Axilrod-Teller C9 (1.52138), coupled dipole characteristic frequency (1.09696), and the repulsive damping coefficient (3.330)

Helium	ϵ (K)	σ/ρ (Å)	C_6	C_8	C_{10}
PHAHST	4.52652	2.38592	1.50167	11.88425	115.21474
AT	4.52700	2.38595	1.50147	11.88266	115.19920
C-D	4.52652	2.38592	-	11.88425	115.21474
LJ	8.32118	2.65208	-	-	-

Table 2: Neon model parameters. Special parameters not listed include Axilrod-Teller C9 (11.85842), coupled dipole characteristic frequency (1.24456), and the repulsive damping coefficient (3.160)

Neon	ϵ (K)	σ/ρ (Å)	C_6	C_8	C_{10}
PHAHST	4.47889	2.80703	6.11081	66.87100	896.43297
AT	4.47880	2.80704	6.11093	66.87232	896.45066
C-D	4.47889	2.80703	-	66.87100	896.43297
LJ	0.38230	29.88995	-	-	-

4 Results and Discussion

Potential Energy Surfaces

The total potential energy surfaces illustrate the robustness of the PHAHST potentials when compared to electronic structure, almost quantitatively reproducing the total energy curve from TZ/QZ coupled cluster. It should be noted that though the blue dotted line associated with the 5Z/6Z energies in the trimer surfaces are a higher level set of basis sets, the helium and neon models used to compare to them were fit to the TZ/QZ dimer and should be compared to them as such. The 5Z/6Z surface was merely a comparison to what the true answer might look like in comparison. It can be seen that while the PHAHST family of potentials reproduce the shape of the *ab initio* better than the Lennard-Jones surface treated as a control, they still slightly underestimate the attractive magnitude of the atomic interactions at the well minimum. Though not pictured, these potentials come to almost exact agreement at both the short- and long-range limits (well within 0.1 K).

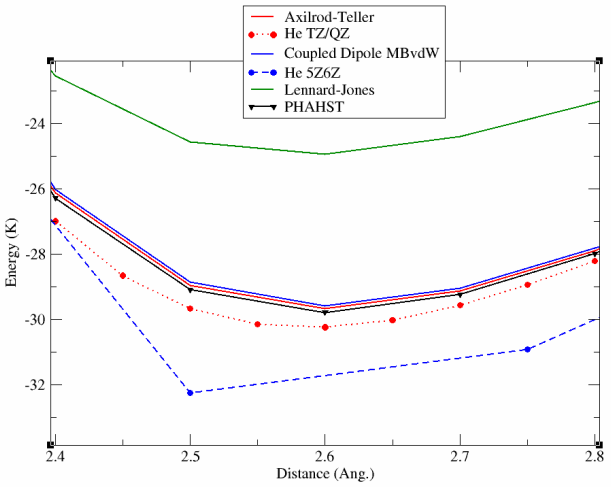

(a) $He_2 + He$

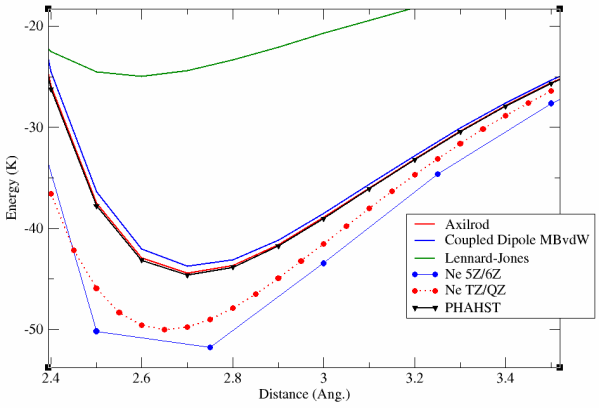

(b) $He_2 + Ne$

Figure 3: Noble gas trimer configuration of classical potential energy surfaces against the coupled cluster energy surface.

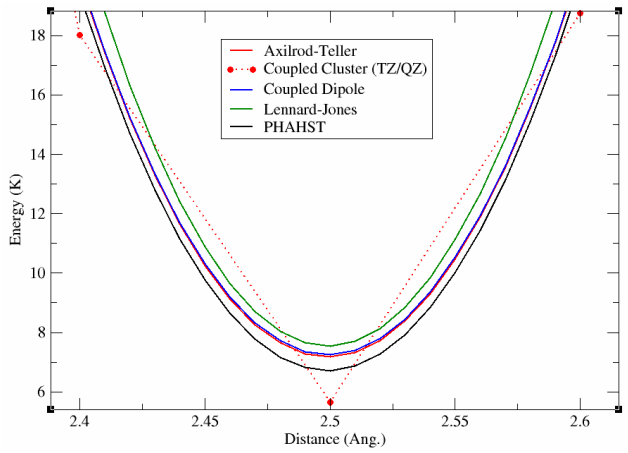

(a) Interior of the nanostructure

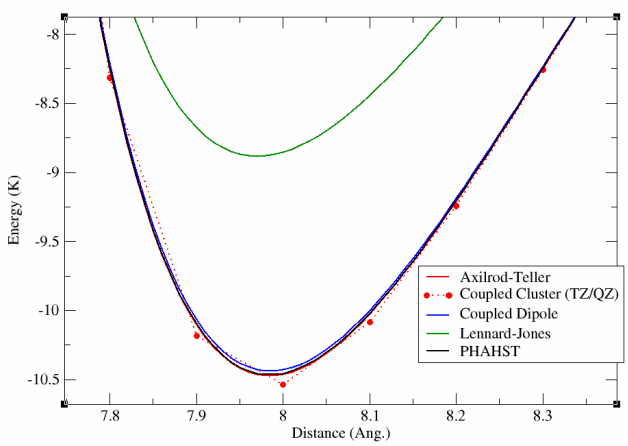

(b) Exterior of the nanostructure

Figure 4: The classical potential energy surfaces compared to CCSD(T) on both the inside and outside of the cage nanostructure.

This disagreement of absolute energy at the minimum is not as important as the first derivative of the surface, however, as in a molecular simulation the gradient of the potential is what will define the force the atoms experience. In the total potential energy curves presented in this work, the agreement between *ab initio* gradient and that of the classical potentials is almost numerically the same, especially when considered against the historically used Lennard-Jones potential form when fit to the same training data.

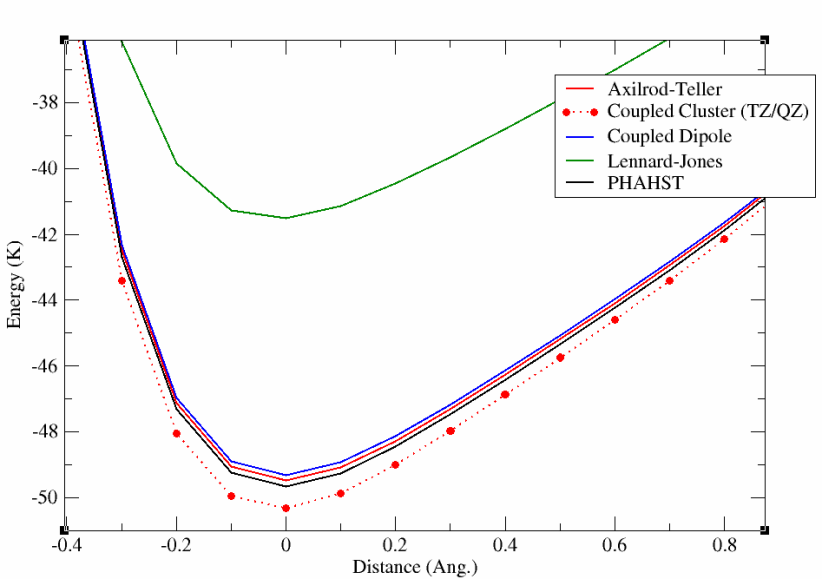

Figure 5: The pocket nanostructure PES.

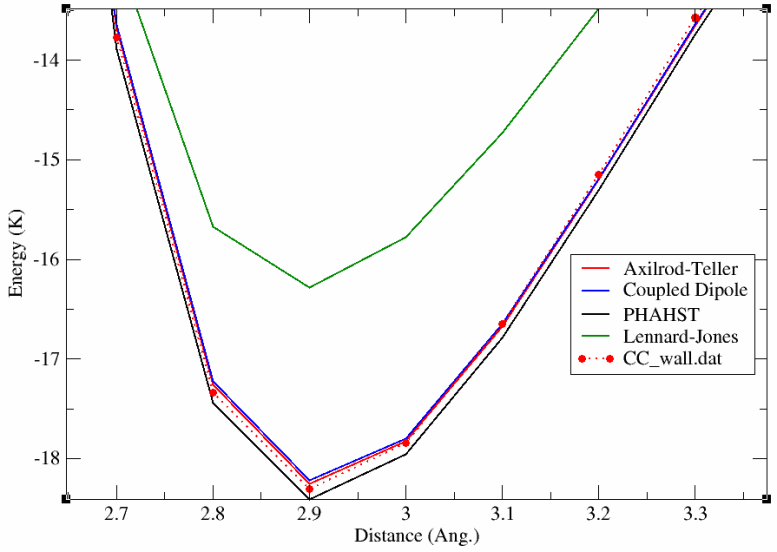

Figure 6: The wall nanostructure PES.

Many-Body Energy Decomposition

When the total energy of each of the nanostructure surfaces are decomposed into their many-body contributions, it is shown that the majority of the total energy is given by the pairwise additive terms, whereas the many-body effects are remarkably weaker by comparison. Note that in the figures below, the scale of the decomposed many-body energy is in units of microkelvin. In almost all cases, the electronic structure values for the total many-body energy contributions are very small when compared to the pair energies, made even smaller because of the alternating sign on subsequently increasing-order terms, e.g. negative 3-body energy, positive 4-body energy, -negative 5-body energy, etc.

It can be shown that the majority of the many-body energy depicted in figures 7-10 is captured by the classical Axilrod-Teller 3-body term when compared to the coupled-dipole many-body correction term. In the instances presented, this serves as a useful guide for describing when it is appropriate to use these corrections and theoretically when the coupled-dipole correction might be needed in the place of the Axilrod-Teller correction. It should be considered however that given the highly symmetric nature of the nanostructures and sorbate-path considered, the difference between the two corrections might be underdetermined, as these configurations are likely prone to a cancellation of opposing attractions or repulsions from a mirrored counterpart within each nanostructure.

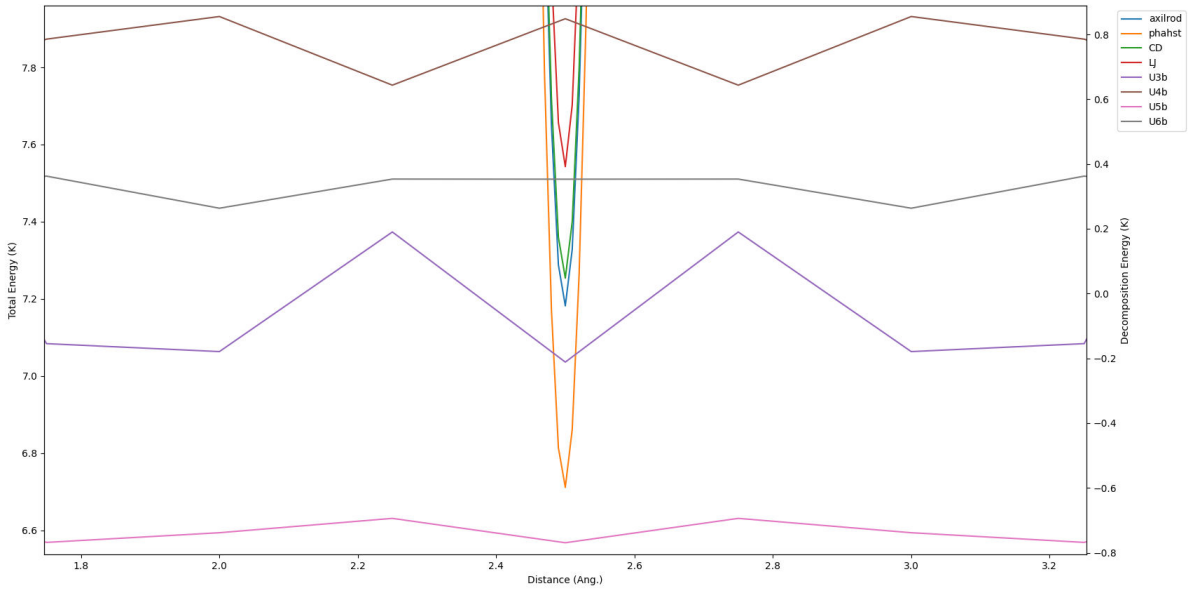

Figure 7: The inside of the cage nanostructure energy decomposition using aug-cc-pVTZ/QZ basis sets compared to classical potentials.

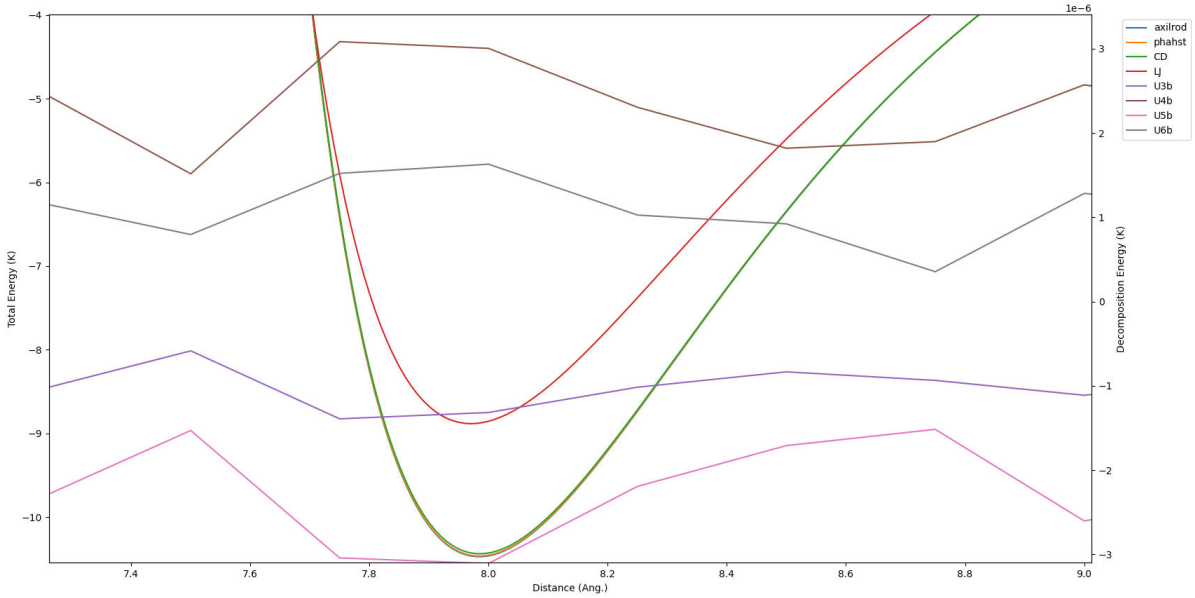

Figure 8: The outside of the cage nanostructure energy decomposition using aug-cc-pVTZ/QZ basis sets compared to classical potentials.

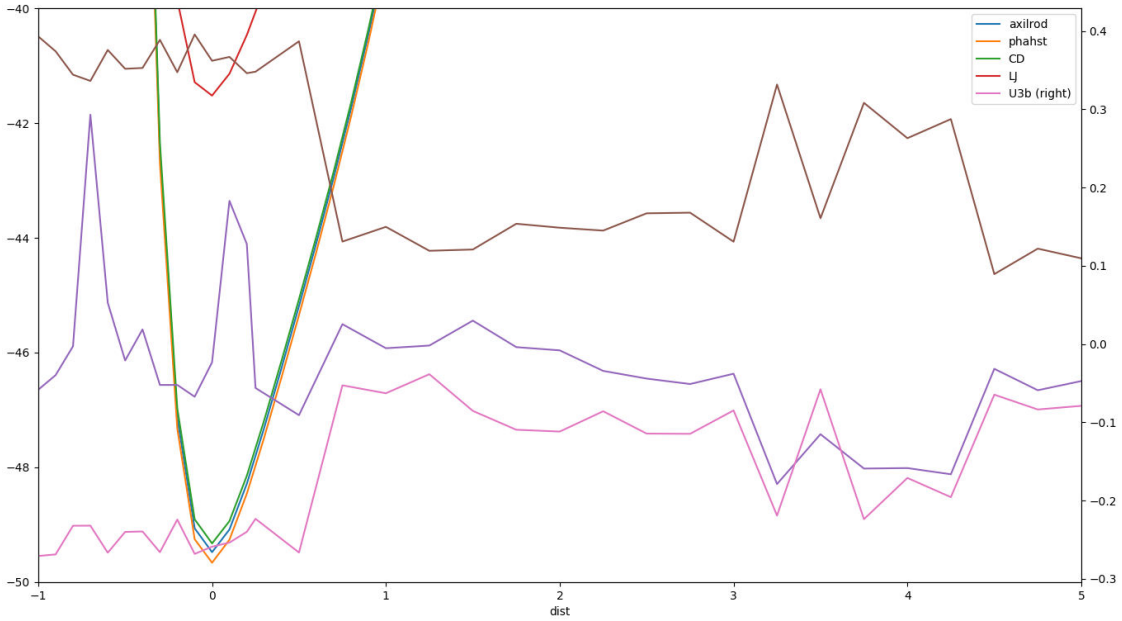

Figure 9: The pocket nanostructure energy decomposition using aug-cc-pVTZ/QZ basis sets compared to classical potentials.

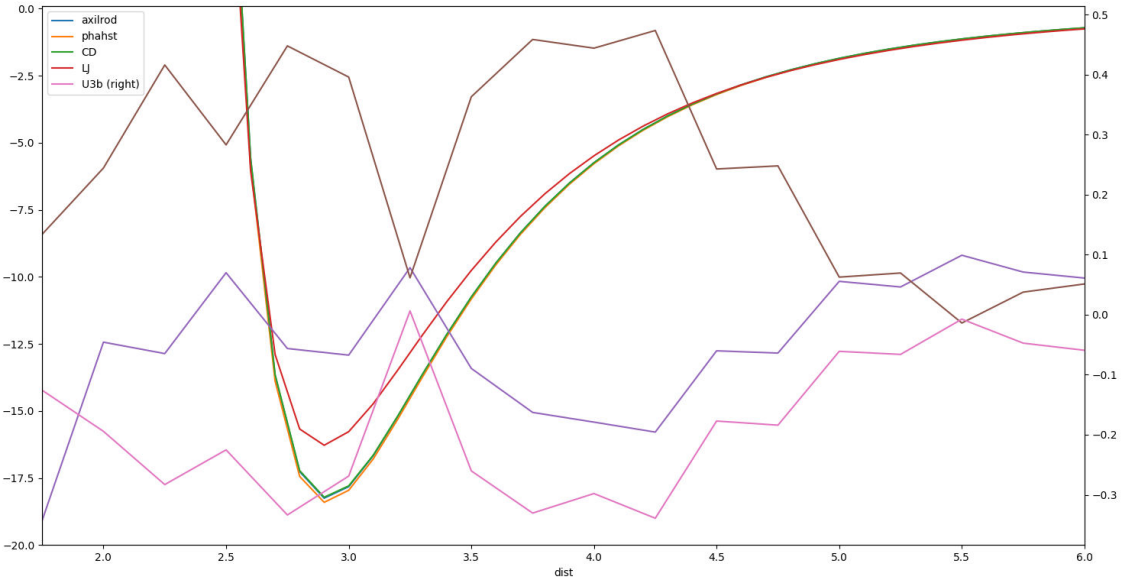

Figure 10: The wall nanostructure energy decomposition using aug-cc-pVTZ/QZ basis sets compared to classical potentials.

5 Conclusions

A novel repulsion-dispersion form has been developed (PHAHST) that accurately reproduces the energetics of induced-polar interactions between van der Waals-dominated chemical species. It is shown that a physically grounded model of exponential repulsion and damped Tang-Toennies style dispersion forces provide a robust and computationally affordable potential form that provides for high accuracy in all of the chemically relevant distance regimes. Model verification of the fit from the coupled cluster dimer was performed against the coupled cluster nanostructures including the cage, pocket, and wall motifs.

It is important to note that the success of a classical potential form which reproduces the Born-Oppenheimer surfaces of the Schrodinger equation solutions for these nanostructures was not guaranteed at the outset of making the PHAHST family of models. That there seem to be potentials that exist which do reproduce these electronic structure results with good accuracy for systems larger than a dimer or trimer is promising for the prospect of investigating much larger systems, namely porous materials and biological systems.

Future Work

Further studies will focus on the exploration of mixing rules in a similarly physically grounded way as the previously talked about aspects of PHAHST. An additional nanostructure not listed here will be included: a ring structure resembling a corridor that might be found in a porous material. As to the choice of further sorbate parameterization in the PHAHST family of potentials, methane is a natural extension to small, spherical, dispersion-dominated chemical species, as its polar moments are small and its structure resembles that of a sphere when the van der Waals surface is considered.

Acknowledgements

I would like to express my sincere gratitude to my supervisor and mentor, Dr. Brian Space. He has remained a consistent and reliable source of guidance both within the lab and beyond.

I would also like to acknowledge Adam Hogan for offering to me his persistent attention to detail and willingness to respond to questions whose answers are generally not simple or convenient to explain.

My good friend Luciano Laratelli, without whom I might very well still be calculating many-body energies in Excel. The value of his help in writing Python scripts has been incalculable, even using double floats.

And to Meagan Mulcair, my partner, editor, and scientific confidante. Her presence and encouragement have been a bulwark against the tempests of stress and self-doubt, without which I could not have finished.

And to the other members of the Space lab, past and present, in particular Chris Cioce, whose idea was the basis for this project.

6 References

(1) Bcs, *Materials for Separation Technologies: Energy and Emission Reduction Opportunities Industrial Technologies Program*; 2005.

(2) Kadioglu, O.; Keskin, S. Efficient separation of helium from methane using MOF membranes. *Separation and Purification Technology* **2018**, *191*, 192–199.

(3) Liu, Y.; Liu, J.; Hu, J. Noble gas separation by a MOF with one-dimensional channels. *BMC Chemical Engineering* **2019**, *1*, 1–7.

(4) Mohamed, M. H.; Elsaidi, S. K.; Pham, T.; Forrest, K. A.; Schaef, H. T.; Hogan, A.; Wojtas, L.; Xu, W.; Space, B.; Zaworotko, M. J.; Thallapally, P. K. Hybrid Ultra-Microporous Materials for Selective Xenon Adsorption and Separation. *Angewandte Chemie* **2016**, *128*, 8425–8429.

(5) Batten, S. R.; Neville, S. M.; Turner, D. R. *Coordination Polymers*; Royal Society of Chemistry: Cambridge, 2008.

(6) Kitagawa, S.; Kitaura, R.; Noro, S. I. Functional porous coordination polymers. 2004; `https://onlinelibrary.wiley.com/doi/full/10.1002/anie.200300610https://onlinelibrary.wiley.com/doi/abs/10.1002/anie.200300610https://onlinelibrary.wiley.com/doi/10.1002/anie.200300610`.

(7) Perry, J. J.; Perman, J. A.; Zaworotko, M. J. Design and synthesis of metal–organic frameworks using metal–organic polyhedra as supermolecular building blocks. *Chemical Society Reviews* **2009**, *38*, 1400–1417.

(8) Eddaoudi, M.; Moler, D. B.; Li, H.; Chen, B.; Reineke, T. M.; O'Keeffe, M.; Yaghi, O. M. Modular chemistry: Secondary building units as a basis for the design of highly porous and

robust metal-organic carboxylate frameworks. *Accounts of Chemical Research* **2001**, *34*, 319–330.

(9) Rappé, A. K.; Casewit, C. J.; Colwell, K. S.; Goddard, W. A.; Skiff, W. M. UFF, a Full Periodic Table Force Field for Molecular Mechanics and Molecular Dynamics Simulations. *Journal of the American Chemical Society* **1992**, *114*, 10024–10035.

(10) Vanommeslaeghe, K.; Hatcher, E.; Acharya, C.; Kundu, S.; Zhong, S.; Shim, J.; Darian, E.; Guvench, O.; Lopes, P.; Vorobyov, I.; Mackerell, A. D. CHARMM general force field: A force field for drug-like molecules compatible with the CHARMM all-atom additive biological force fields. *Journal of Computational Chemistry* **2010**, *31*, 671–690.

(11) Pearlman, D. A.; Case, D. A.; Caldwell, J. W.; Ross, W. S.; Cheatham, T. E.; DeBolt, S.; Ferguson, D.; Seibel, G.; Kollman, P. AMBER, a package of computer programs for applying molecular mechanics, normal mode analysis, molecular dynamics and free energy calculations to simulate the structural and energetic properties of molecules. *Computer Physics Communications* **1995**, *91*, 1–41.

(12) Hogan, A.; Space, B. Next-Generation Accurate, Transferable, and Polarizable PHAHST Potentials For Material Simulations. *JCTC* **2020**, *Unpublishe*.

(13) Axilrod, B. M.; Teller, E. Interaction of the van der Waals type between three atoms. *The Journal of Chemical Physics* **1943**, *11*, 299–300.

(14) Cole, M. W.; Velegol, D.; Kim, H. Y.; Lucas, A. A. Nanoscale van der Waals interactions. Molecular Simulation. 2009; pp 849–866.

(15) Kim, H.-Y. *An Efficient Coupled Dipole Method for the Accurate Calculation of van der Waals Interactions at the Nanoscale*; Springer, Singapore, 2015; pp 85–119.

(16) McLaughlin, K.; Cioce, C. R.; Belof, J. L.; Space, B. A molecular H 2 potential for heteroge-

neous simulations including polarization and many-body van der Waals interactions. *Journal of Chemical Physics* **2012**, *136*, 194302.

(17) Neese, F. The ORCA program system. *Wiley Interdisciplinary Reviews: Computational Molecular Science* **2012**, *2*, 73–78.

(18) Neese, F. Software update: the ORCA program system, version 4.0. *Wiley Interdisciplinary Reviews: Computational Molecular Science* **2018**, *8*.

(19) Kendall, R. A.; Dunning, T. H.; Harrison, R. J. Electron affinities of the first-row atoms revisited. Systematic basis sets and wave functions. *The Journal of Chemical Physics* **1992**, *96*, 6796–6806.

(20) Wilson, A. K.; Van Mourik, T.; Dunning, T. H. Gaussian basis sets for use in correlated molecular calculations. VI. Sextuple zeta correlation consistent basis sets for boron through neon. *Journal of Molecular Structure: THEOCHEM* **1996**, *388*, 339–349.

(21) Truhlar, D. G. Basis-set extrapolation. *Chemical Physics Letters* **1998**, *294*, 45–48.

(22) Chaudhuri, P.; Canuto, S. Many-body energy decomposition of hydrogen-bonded glycine clusters in gas-phase. *Chemical Physics Letters* **2010**, *491*, 86–90.

(23) Franz, D. M.; Belof, J. L.; McLaughlin, K.; Cioce, C. R.; Tudor, B.; Hogan, A.; Laratelli, L.; Mulcair, M.; Mostrom, M.; Navas, A.; Stern, A. C.; Forrest, K. A.; Pham, T.; Space, B. MPMC and MCMD: Free High□Performance Simulation Software for Atomistic Systems. *Advanced Theory and Simulations* **2019**, *2*, 1900113.

(24) Casimir, H. B.; Polder, D. The influence of retardation on the London-van der Waals forces. *Physical Review* **1948**, *73*, 360–372.

(25) Barton, D. E.; Abramovitz, M.; Stegun, I. A. *Journal of the Royal Statistical Society. Series A (General)*; Dover Publica- tions, Inc: Mineola, NY, 1965; Vol. 128; Chapter 25, Sect., p 593.

(26) Fuchs, R. R.; McCourt, F. R.; Thakkar, A. J.; Grein, F. Two new anisotropic potential energy surfaces for N2-He: The use of hartree-fock SCF calculations and a combining rule for anisotropic long-range dispersion coefficients. *Journal of Physical Chemistry* **1984**, *88*, 2036–2045.

(27) Mullen, A. L.; Pham, T.; Forrest, K. A.; Cioce, C. R.; McLaughlin, K.; Space, B. A polarizable and transferable PHAST CO2 potential for materials simulation. *Journal of Chemical Theory and Computation* **2013**, *9*, 5421–5429.

(28) Cioce, C. R.; McLaughlin, K.; Belof, J. L.; Space, B. A polarizable and transferable PHAST N2 potential for use in materials simulation. *Journal of Chemical Theory and Computation* **2013**, *9*, 5550–5557.

(29) Thole, B. T. Molecular polarizabilities calculated with a modified dipole interaction. *Chemical Physics* **1981**, *59*, 341–350.

(30) Shukla, N.; Arora, B.; Sharma, L.; Srivastava, R. *Two-dipole and three-dipole dispersion coefficients for interaction of alkaline-earth atoms with alkaline-earth atoms and alkaline-earth ions*; 2020.

(31) Midzuno, Y.; Kihara, T. Non-additive Intermolecular Potential in Gases I. van der Waals Interactions. *Journal of the Physical Society of Japan* **1956**, *11*, 1045–1049.

(32) Bade, W. L.; Kirkwood, J. G. Drude-model calculation of dispersion forces. II. The linear lattice. *The Journal of Chemical Physics* **1957**, *27*, 1284–1288.

(33) Jensen, L.; Åstrand, P. O.; Sylvester-Hvid, K. O.; Mikkelsen, K. V. Frequency-dependent molecular polarizability calculated within an interaction model. *Journal of Physical Chemistry A* **2000**, *104*, 1563–1569.

(34) Misquitta, A. J.; Stone, A. J. Distributed polarizabilities obtained using a constrained density-fitting algorithm. *Journal of Chemical Physics* **2006**, *124*, 024111.

(35) Misquitta, A. J.; Stone, A. J. Accurate induction energies for small organic molecules: 1. Theory. *Journal of Chemical Theory and Computation* **2008**, *4*, 7–18.

(36) Stone, A. J.; Misquitta, A. J. Atom-atom potentials from ab initio calculations. 2007; `https://www.tandfonline.com/doi/abs/10.1080/01442350601081931`.